Title

Laser Ultrasonic Imaging of Wavefield Spatial Gradients for Damage Detection

ISBN

9789811591983

Authors

Chong, SY

Wu, Z

Todd, MD

Publication Date

2021

DOI

10.1007/978-981-15-9199-0_63

Peer reviewed

Laser Ultrasonic Imaging of Wavefield Spatial Gradients for Damage Detection

S. Y. Chong[1], Z. Wu[1], and M. D. Todd[†]

[1,†]*Department of Structural Engineering, University of California San Diego, 9500 Gilman Drive, La Jolla CA 92093-0085, USA.*

[†]*E-mail: mdtodd@eng.ucsd.edu*

Abstract

Laser ultrasonic techniques (LUTs) are increasingly used in non-destructive evaluation (NDE) applications because they can provide full-field ultrasonic wavefield data with high resolution in a three-dimensional (3D) space-time domain. This paper investigates the properties of the wavefield *spatial gradient* as a detector and localizer for defects that distort the local wavefield. A laser ultrasonic interrogation method based on a 527-nm Q-switched laser scanning system was used to interrogate 3D ultrasonic signals in a 3-mm aluminum plate. The plate was tested with and without multiple artificial scatterers to test the proposed method. During the scanning process, the ultrasonic waves were generated by the pulsed laser at an *n*-by-*m* grid of sampling points and recorded by a single fixed PZT transducer. The whole scan generates a 3D matrix which allows the accessibility of showing the wave propagation over time in movie form with a high spatial resolution. After the scanning process, the full-field ultrasonic data of the plate without and with artificial damage were obtained, respectively. Then, spatial gradient vectors were computed from each frame of the full-field ultrasonic data along the time axis. For a space-domain frame $\{U_i\}^{n\times m}$ at a time $i \in t$, the gradient vectors were determined by two components, $\{G_{i,x}\}^{n\times m}$ and $\{G_{i,y}\}^{n\times m}$, which reflected the spatial derivatives of every pixel with respect to the position coordinates. Once the gradient vectors of the full-field ultrasonic data (intact and damage cases) were determined, the spatial-gradient ultrasonic wavefield imaging was generated with the gradient orientation profile $\{\theta_i\}^{n\times m}$ and the gradient magnitude profile $\{A_i\}^{n\times m}$ as the features used for damage detection. The wavefield spatial gradients of the defect-free case were used as a baseline to compare with the wavefield spatial gradients of the damaged case. The gradient profiles of the wavefield spatial gradients could detect and localize the damage by the inconsistency of the wave pattern in the 2D space domain. The wavefield spatial gradients also showed the ability to remove the complexity of identifying the damage among multi-mode waveform. Future work will be focusing on applying the algorithm to complex structures such as CFRP composites.

Keywords: Guided waves, Laser ultrasonics, Wavefield imaging, Non-destructive evaluation, Spatial gradient analysis

1 Introduction

Laser ultrasonic techniques are increasingly used in non-destructive evaluation applications because they can provide full-field ultrasonic wavefield data with high spatio-temporal resolution. The full-field ultrasonic wavefield data is generally formed via 3D imaging techniques, known as ultrasonic wavefield imaging (UWI). Obtaining the UWI directly with such a high resolution (and extracting certain features) gives unprecedented insight into how the waves interact with boundaries and how the wavefield may be distorted by scattering from potential defects. With these advantages, many feature-extraction algorithms have been developed based on the temporal- and spatial-frequency transformation methods [1, 2] to detect damage such as fatigue cracks, impacts, and corrosion. Temporal-correlation [3] and spatial-covariance [4, 5] methods were developed as well to detect and localize the damage.

Beyond these features mined from the UWI, the wave propagation *orientation* of the ultrasonic wavefield has not been considered in ultrasonic interrogation. Since the UWI is formed in 3D space-time domain, 2D *spatial gradient field* can be determined in each time frame. Since boundary or material changes are known to induce changes in spatial ultrasonic field properties, it may then be reasonably further surmised that defects may be detected by monitoring the change of the spatial gradient field as time progresses.

Many spatial gradient field analyses are used in seismic and image recognition applications. In seismic applications, the spatial gradient of the seismic wavefield is analyzed to investigate important wave characteristics that can be directly related to wave propagation in layered earth [6]. In image recognition applications, the spatio-temporal gradient method is used to recognize a moving object in video data [7]. Hence, it suggests the hypothesis that the change of the local spatial gradient of the UWI may be detected through the spatial gradient analysis method to the ultrasonic wavefield imaging.

In this paper, we propose a wavefield spatial gradient analysis method to laser ultrasonic imaging for damage detection. First, the spatial gradient analysis method to the laser ultrasonic imaging is presented. Then, the experimental setup to obtain the full-field ultrasonic wavefield data from the specimen with and without artificial defects is discussed. Lastly, the detectability of the proposed method on multiple simultaneous defects is discussed.

2 Ultrasonic Wavefield Spatial Gradients

The proposed method is based on acquiring the gradient-orientation and the gradient-magnitude profiles along with time history. To evaluate the presence of potential defects, the 2D spatial gradient vectors of each time frame (denoted as *i*-index) are calculated and the corresponding gradient vector components may be expressed by

$$\{G_{i,x}\}^{n\times m} = \frac{\partial U_i}{\partial x}, \quad \{G_{i,y}\}^{n\times m} = \frac{\partial U_i}{\partial y}, \tag{1}$$

which represent the differences for each pixel of $\{U_i\}^{n\times m}$ in the *x* (horizontal) and *y* (vertical) directions, respectively. The spacing between pixels in each direction is adjusted with the expected spatial resolution. Based on the Eqn. (1), the gradient-orientation and gradient-magnitude profiles for each time frame, $\{\theta_i\}^{n\times m}$ and $\{A_i\}^{n\times m}$, can be determined by the relation of $\theta_i = \tan^{-1}(G_{i,y}/G_{i,x})$ and $A_i = \sqrt{G_{i,x}^2 + G_{i,y}^2}$, respectively. Thus, by integrating the variations of these spatial gradient's

components with the sampled time, *i*, the gradient-orientation and gradient-magnitude maps of the full-field ultrasonic wave can be generated

$$\left\{G_\theta\right\}^{n\times m}=\sum_{i=1}^{t_{end}-1}\left[\left\{\theta_{i+1}\right\}-\left\{\theta_i\right\}\right], \text{and } \left\{G_A\right\}^{n\times m}=\sum_{i=1}^{t_{end}-1}\left[\left\{A_i\right\}\right], \tag{2}$$

respectively. Consequently, these maps may detect and visualize the damaged area with a change from approximately low accumulation to high accumulation. However, the spatial gradient vectors are sensitive to the reflected waves, too, of course. The reflected wave may make these maps fail to distinguish the defects located near the boundary of the specimen. Given that, a scanning result of the defect-free case, $\left\{U_{i,0}\right\}^{n\times m}$, is considered and pre-recorded as a baseline and the gradient-orientation and gradient-magnitude maps obtained from $\left\{U_{i,0}\right\}^{n\times m}$ are defined as the residual gradient-orientation map $\left\{G_{\theta,0}\right\}^{n\times m}$ and the residual gradient-magnitude map $\left\{G_{A,0}\right\}^{n\times m}$, respectively. For that, ideally, the effect of the reflected wave can be removed by subtracting the baseline from the damaged data expressed in the following form:

$$\left\{G_{\theta,\text{sub}}\right\}^{n\times m}=\left\{G_\theta\right\}^{n\times m}-\left\{G_{\theta,0}\right\}^{n\times m}, \text{ and } \left\{G_{A,\text{sub}}\right\}^{n\times m}=\left\{G_A\right\}^{n\times m}-\left\{G_{A,0}\right\}^{n\times m}, \tag{3}$$

where the $\left\{G_{\theta,\text{sub}}\right\}^{n\times m}$ and $\left\{G_{A,\text{sub}}\right\}^{n\times m}$ are the residual trajectories caused by the defects. Both residual maps may have different damage detection patterns which can be further interpreted to localize the damages according to their sensitivities to different types of damages. In this paper, the circle scanning data was considered, and the space-domain *n*-by-*m* frame (*x*- and *y*-directions) corresponds with the dimension defined by total inspection scan angle points and total inspection scan radius points in the Cartesian coordinate scheme. The angular direction of the damage can be accurately determined in light of the spatial covariance method [4, 5].

3 Experimental Setup

Figure 1(a) shows a schematic diagram of a laser ultrasonic interrogation system (LUIS). This system consists of a laser scanning system incorporated with a signal conditioning device, a data acquisition (DAQ) module, a contact sensor, and a computer used for signal processing and operation control.

The laser scanning system has a two-dimensional laser scanner and a diode-pumped solid-state Q-switched Nd:YAG laser. The Q-switched laser is composed of a laser controller and a laser head with an output beam of 527 nm wavelength and pulse repetition rates (PRR) from single-shot to 1 kHz. The

2D laser scanner is used to synchronize the 2-axis galvanometer scanner (Fig. 1(b)) with the Q-switched laser to maneuver the laser impinging point rapidly on a target at a PRR according to the preset scanning pattern coordinates. As for this paper, the circle scanning pattern was considered, and the ultrasounds were generated and obtained at each coordinate of (R,θ) in the polar coordinate space. The scanning radius ranges were set from 20 mm to 220 mm with an interval of 0.5 mm, and the angular interval was set to 0.26°.

During the scanning process, a laser pulse impinges at a scan point, and the corresponding ultrasound is generated at the local point based on the thermoelastic principle. The generated ultrasound is then signal-conditioned through a contact sensor and digitized in the DAQ module as shown in Fig. 1(a). In the DAQ module, the generated ultrasound is digitized synchronously with the PRR of the laser scanning system by receiving a triggering signal from the laser controller after the laser pulse is emitted. In the digitizing process, the ultrasound is sampled for K number of data points (each sample point is denoted as index i) at sampling time interval T_S and stored in a computer. The digitizing process is repeated as the scanning process is performed. In this paper, the K was set to 2000 at the sampling interval of $T_S = 0.2$ μs.

Lastly, all digitized ultrasonics are represented in the form of a three-dimensional R-θ-T matrix, indexed by spatial-horizontal-direction (m), spatial-vertical-direction (n), and i time samples, respectively, along with each dimension. In this paper, two different notations of 2D Cartesian coordinates scheme were used for the $\{U_i\}^{n\times m}$ obtained from the polar scan. One was presented in the R-θ domain, and the other one was presented in the X-Y domain. The corresponding coordinates of X and Y axes were simply determined by the relationships of $X = R\cos\theta$ and $Y = R\sin\theta$ respectively. For example, Fig. 1(c) shows the snapshot of an ultrasonic wavefield image at 82 μs, representing in X-Y domains.

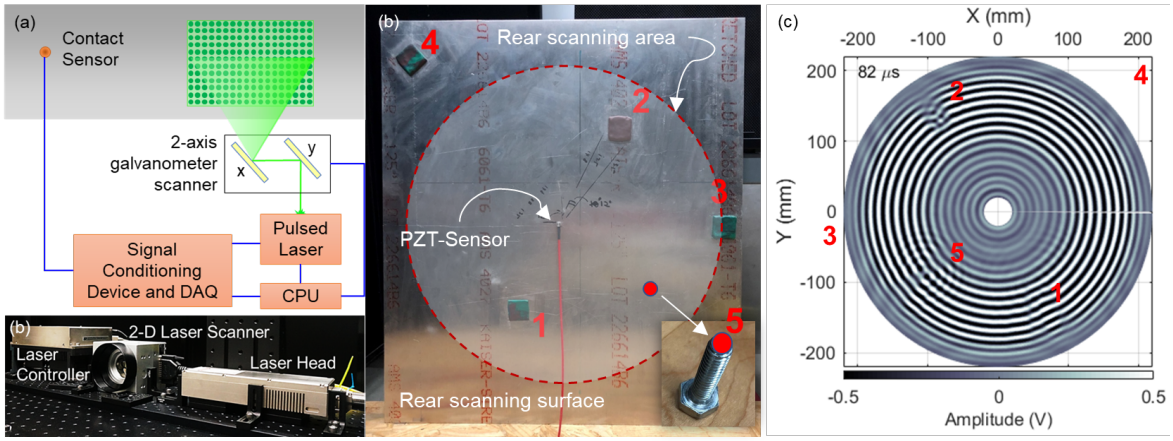

Figure 1: (a) Laser ultrasonic interrogation system configuration, (b) 3-mm aluminum plate configurations with simulating defects, and (c) ultrasonic wavefield image at 82 μs.

Figure 1(b) shows the defect types and locations as considered for the multiple damage scenarios. Four scanning processes were performed. First, the specimen without any defects was considered and used as a baseline for the damage detection. Second, the single damage case was considered with plasticine at location 2. Third, the multi-location damage case with plasticine at location 1 to 4 as shown in Fig. 1(b). Last, the multi-type damage case was considered by including a screw (inset of Fig. 1(b)), where the red surface was glued on the rear scanning surface at location 5.

4 Results and Discussion

4.1 Single Damage Case

The proposed method is firstly demonstrated for a single damage case. A piece of plasticine (20 mm × 20 mm) was bonded at location 2 of the aluminum plate by grew acting as a damper to the guided waves. Figure 2(a) shows the ultrasonic wavefield image at 60 μs. The attenuated local amplitudes of the A0 mode were barely visible at the damage location. In contrast, the gradient-orientation map (2), as shown in Fig. 2(b), was able to detect and localize the damage at location 2 with the Cartesian coordinate of (–95, 125). Then, the angular direction of the damage was also accurately determined at 125° using the spatial covariance method [4, 5] to the gradient-orientation map, as shown in Fig. 2(c).

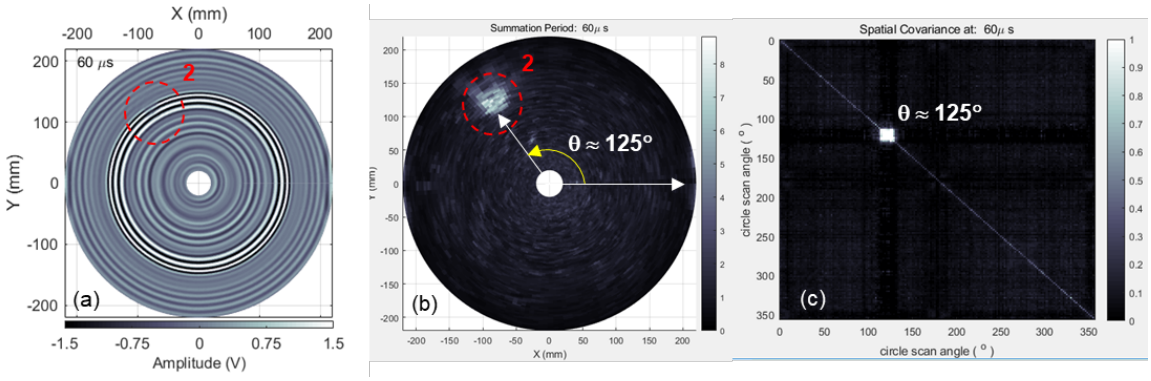

Figure 2: (a) UWI at 60 μs, (b) gradient-orientation map for the single-damage case, and (c) the corresponding angle covariance of the gradient-orientation map obtained from circle scanning.

However, even though the damaged area was detected in the gradient-orientation map with a change in variation summation from approximately zero value to a higher accumulation, the methodology is extremely limited by the incident wave because the presence of the reflected wave, after the time of 60 μs, distorts the consistency of the guided wave and make the undamaged area that near the boundary have a higher accumulation, as shown in Fig. 3(a) at 64 μs. Figure 3(b) shows the false positive on the covariance map which due to the reflected waves. Thus, the baseline subtraction method was considered and showed the ability to detect the damage as showed in Fig. 3(c). Figure 3(c) shows the gradient-

orientation map is able to indicate the location of the damage even furthermore the time span (> 60 μs) where the reflected waves were starting propagated toward to the center plate.

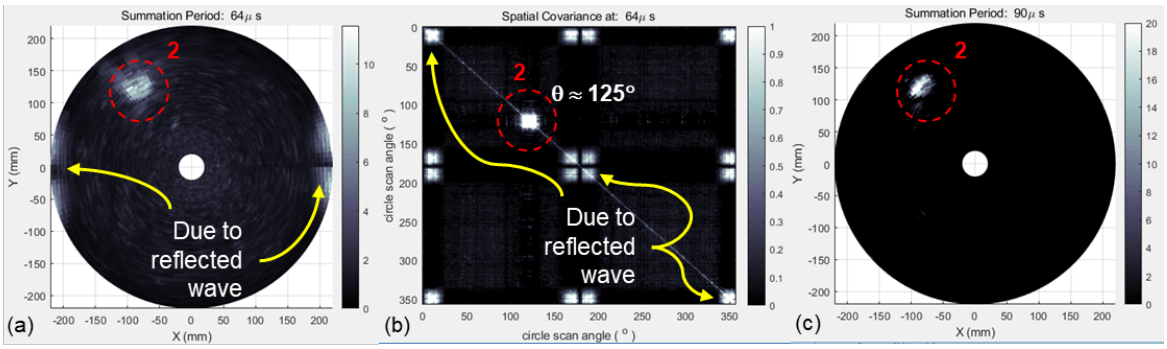

Figure 3: (a) gradient-orientation map for the single-damage case at 64 μs, (b) the corresponding angle covariance of the gradient-orientation map, and the residual gradient-orientation map based on baseline method at 90 μs.

4.2 Multi-location Damage Case

The multi-location damage case with three artificial plasticine pieces including one near the plate boundary was conducted to evaluate the feasibility of the proposed method after removing the reflected wave limitation through the baseline subtraction. Figures 4(a) and (b) show that all three simulating defects were detected in the gradient-orientation map clearly at the time 120 μs. However, there were false-positive detected regions (Fig. 4(a)) caused by the scattering effect of the damage (location 1). In this case, the defect at location 4, which is outside the scanning area (Fig. 1(b)), was not be able to be detected.

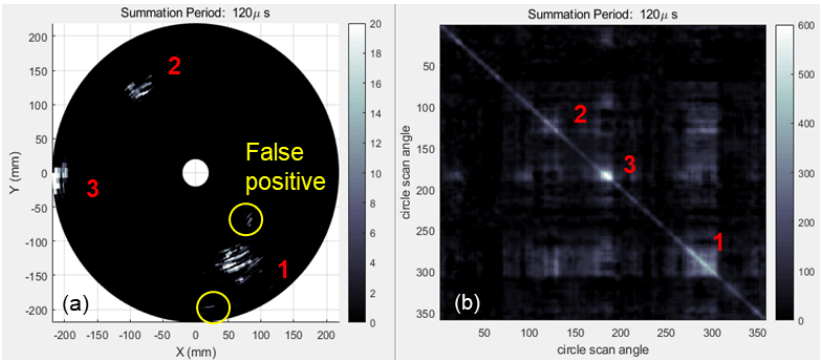

Figure 4: Multi-location damage case: (a) Residual gradient-orientation map with baseline subtraction (reflected wave removed), and (b) corresponding angle covariance of the residual gradient-orientation map obtained from circle scanning.

4.3 Multi-type Damage Case

In this case, a screw was bonded in the mark location 5, as shown in Fig. 1(b), acting as a scattering source to evaluate the gradient-magnitude map result. The gradient-magnitude map (3), as shown in Fig. 5(a), was able to detect and localize the multi-type and multi-location damages (at location 1, 2, 3, and 5) with the polar scan coordinates. The magnitude-based map is converted into Cartesian coordinate as a more intuitive view. The angular direction of the damages was again accurately determined at 125°, 180°, 220°, and 295° using the spatial covariance method to the gradient-magnitude map, as shown in Fig. 5(c). The four trajectories with distinct patterns in this map indicate the change of the wavefield caused by the four artificial defects in the experimental case. With the angle indicated by the corresponding angle covariance map (Fig. 5(c)), the damages can be located by the peak value for each trajectory.

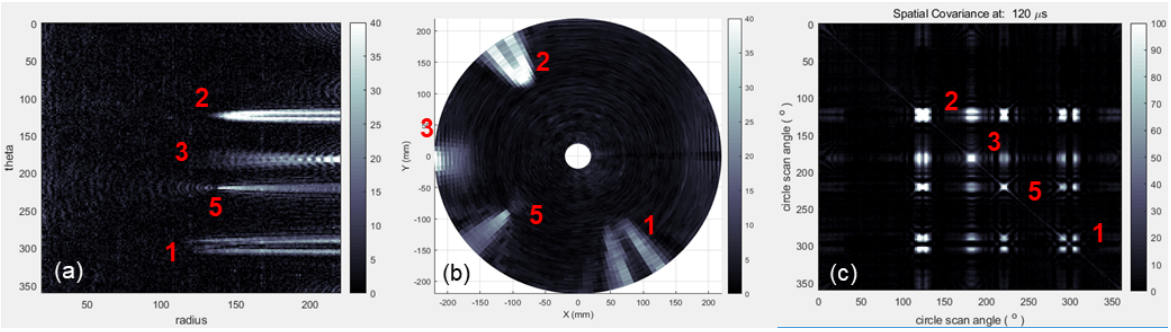

Figure 5: Multi-type damage case: Residual gradient-magnitude map on (a) R-θ axes and (b) x-y axes with baseline subtraction, and (c) corresponding angle covariance of the residual gradient-magnitude map.

5 Conclusion

In this paper, the laser ultrasonic imaging of the wavefield spatial gradients for damage detection was proposed. The ultrasonic wavefield spatial gradient analysis method with the gradient-magnitude and gradient-orientation maps were presented and used to detect the damages by monitoring the change in the components of the spatial gradient vector. Then, the proposed method was tested on the ultrasonic wavefield imaging that obtained from the aluminum plate with four different configurations of the artificial damages. In the first case, the gradient-orientation map showed the ability to detect the single damage but only limited to using the incident waves. The presence of the reflected waves made the map difficult to distinguish between changes due to the scattering waves from the damage and the reflected waves from the plate boundaries. To address that, the baseline subtraction method was considered to suppress the effects of the reflected wave. Then, the residual gradient-orientation map obtained by the baseline subtraction was tested on the multiple damages case. It showed the ability to detect the multiple damages, but there was false positive that due to the scattered wave from the damage boundaries. In the last cases, the residual gradient-magnitude map was considered on the multi-type damages. The map was able to identify the distinct patterns due to the damages which were different from the residual gradient-orientation map. The map showed four trajectories with distinct patterns in the map that

indicated the change of the wavefield caused by four artificial defects. Upon that, the spatial covariance of the residual gradient-orientation and gradient-magnitude maps showed the good agreement of the angular directions of the damages respectively. The proposed method showed the detectability of the multiple and multi-type artificial damages even the damage was located at the end of the scanning region (location 3). However, it was not able to detect the damage located outside the scanning region. Future works, the spatial gradient analysis method will be further tested on the complex wavefield patterns, e.g. in the anisotropic material plate-liked structure.

Acknowledgement

The authors acknowledge funding from UC Office of the President for partial support of this work.

References

[1] J.-R. Lee et al., "Laser ultrasonic propagation imaging method in the frequency domain based on wavelet transformation." *Optics and Lasers in Engineering* 49, no. 1 (2011): 167-175.

[2] E. B. Flynn et al., "Structural imaging through local wavenumber estimation of guided waves." *Ndt & E International* 59 (2013): 1-10.

[3] J.-R., C. C. Chia, C.-Y. Park, and H. Jeong, "Laser ultrasonic anomalous wave propagation imaging method with adjacent wave subtraction: algorithm." *Optics & Laser Technology* 44, no. 5 (2012): 1507-1515.

[4] S. Y. Chong, and M. D. Todd, "Dispersion curve estimation via a spatial covariance method with ultrasonic wavefield imaging." *Ultrasonics* 89 (2018): 46-63.

[5] S. Y. Chong, and M. D. Todd, "Statistical damage detection based on full-field covariance of circumferential scan ultrasonic measurement." In *Health Monitoring of Structural and Biological Systems XII*, vol. 10600, p. 106002J. International Society for Optics and Photonics, 2018.

[6] C. Van Renterghem et al., "Spatial wavefield gradient-based seismic wavefield separation." Geophysical Journal International212, no. 3 (2017): 1588-1599.

[7] S.-P. Liou, and R. C. Jain, "Motion detection in spatio-temporal space." Computer Vision, Graphics, and Image Processing 45, no. 2 (1989): 227-250.